Master Thesis Draft
First Edition

1 Introduction

1.1 Overview

Insects have been an important source of inspiration for humans to study and mimic their flight methods [1]. There are various kinds of insects, and most of them fly by fluttering their wings. Their flight muscles can be divided into two types - direct and indirect, which help them to utilize a combination of rotating, flapping, and pitching movements to achieve different wing movements and generate aerodynamic force through various mechanisms.
Insects typically move their wings in a figure-of-eight pattern while hovering, as shown by several studies conducted by researchers such as Amiralaei et al., Fenelon, and Furukawa, among others. A unique tandem wing configuration which has been studied in depth by Sun and Lan Dragonflies is observed in dragonflies flight . They have made significant advancements in 3D flapping wing kinematics by examining the interaction between the fore- and hind-wings.
In the early stages of research, scientists focused on studying the aerodynamics of single-flapping airfoils and combinations of airfoils. They used various techniques such as flow visualization, laser-Doppler velocimetry, panel, and Navier-Stokes computations to analyze the unsteady flows. It is then shown how this flapping-wing database was used to conceive, design and develop a micro air vehicle with a fixed wing for lift and two flapping wings for thrust generation [2].
During the early 20th century, Knoller and Betz proposed a theory concerning the physics of flapping wings. They suggested that an airfoil could be represented as performing harmonic plunge oscillations. This theory was later confirmed by Katzmayr in 1922 when he tested an airfoil in an oscillating wind tunnel flow. Birnbaum further analyzed this effect in 1924 using Prandtl's unsteady thin airfoil theory and was the first to make a quantitative prediction of thrust generation due to slowly oscillating airfoils. He also discovered that oscillating airfoils shed vortices from their trailing edges. Garrick later presented findings in 1936, which were valid for the complete frequency range, based on Theodorsen's thin airfoil theory. Around the same time, von Kármán and Burgers pointed out that the vortex shedding from a thrust-producing oscillating airfoil takes the form of a "reverse" Karman vortex street.
In 1960, Crawford H. Greenewalt presented an important theory [3]. He suggested that the constancy of the wing beat rate in hummingbirds, insects, and birds could be explained as characteristic frequencies of driven damped oscillators. Greenewalt assumed that the motion of such oscillators is harmonic and can be described by the following differential equation ($\dot{\varphi} = d\varphi/dt$, etc.).

$$I\ddot{\varphi} + B\dot{\varphi} + fr = F_0 r \cos(\omega t), \tag{1}$$

where
I is the moment of inertia of the oscillator,
B the damping parameter, which accounts for the external and internal damping resistance assumed to be proportional to the angular velocity of the oscillator,
f the harmonic restoring force,
F_0 the amplitude of the driving force,
r the effective radius of attack of f and F_0
ω the frequency of the driving force ($\omega = 2\pi v$, where v is the number of oscillations per unit time),
φ the angular displacement, and
t time .

After 2000, insect-size drone-micro air vehicles (MAVs) gradually became an active, well-integrated research area, which can perform autonomous flight in natural and man-made environments [4].
Biomimetic design systems associated with flapping Micro Aerial Vehicles (MAVs) can be categorized into four key aspects: flapping mechanism, wing design, manufacturing, and systematic design. There are two crucial issues in the biomimetic MAV design, namely the flapping wing mechanism and weight limitation. High power and high frequency are necessary for the flapping-wing mechanism to create sufficient lift force. Additionally, a light wing-body is essential, which, however, imposes restrictions on the synthesis of the actuators, power sources, or materials, constraining the wing kinematic, frequencies, size, or available aerodynamic forces.

1.2 Resonance

Flapping-wing insects, birds are thought to offset the high power cost of oscillatory wing motion by using elastic elements for energy storage and return. Many insects [5, 6, 7, 8, 9], birds[8, 10] and even bats [11] have spring-like elements in the form of elastic materials in their thoraxes, muscles and tendons to reduce the energetic demands of flapping flight and improve flight efficiency[8] . This system sometimes is called the 'thorax-wing' system. In an ideal situation where elastic components and systems operate at resonance, the kinetic and potential energy of the moving components would be conserved. As a result, power would only be spent on non-conservative energy costs like friction and aerodynamic damping from the wings. Biological evidence such as that in [12] and [3] speculated the 'thorax-wing' system as an oscillator. Based solely on a large amount of observation of different species, Greenewalt[3]claimed that when the muscular driving force is in resonance with the system, the muscular energy consumption is minimized. Another related study by Dudley[13] found that insects' wingbeat frequency is relatively constant, with variations of only 5% during typical hovering flight. They hypothesized that the energetic expenditure is minimised at this relatively constant frequency, which may be the resonant frequency of oscillation.
Therefore, flapping-wing air vehicles can improve efficiency by operating at resonance to reduce the inertial costs of wing acceleration and deceleration. One approach to this objective is to use integrated, compliant mechanisms driven at their resonant frequency. Goldfarb created micro air vehicles (MAVs) with flapping wings that are powered by piezoelectric actuators. These wings are designed to vibrate at a specific frequency known as the resonant frequency[14, 15, 16]. A study conducted by S. Baek[17] analyzed a resonant drive to reduce average battery power consumption used in DC motor-driven flapping-wing robots. They derive a nondimensionalized model of the generic class of a motor-driven slider crank, considering factors such as motor and battery resistance. Agrawal demonstrated a novel, motor-driven four-bar crank-rocker mechanism that integrated a spring to store energy during a flapping cycle [18, 19, 20, 21]. D.faux et al.[22] addresses the design of elastic structures for artificial wings to optimize their dynamic behavior and reproduce insect wing kinematics. As emphasized by Baek et al. [17], at the smallest scales, the principle of mechanical resonance is widely implemented in artificial systems because elasticity is inherently present in both structures and actuators. Few attempts have been made to optimize energy efficiency via elastic elements [17, 18], but the non-linearity of the transmission reduces the benefits of resonance. In 2016, Noah T. Jafferis[23] developed and experimentally verified a non linear damping model of actuation-limited flapping-wing vehicles with passively rotating wing hinges This work inspired J. Zhang and X. Deng[24] modelling the dynamics of the flapping wing as a forced nonlinear resonant system.They employed the nonlinear perturbation method and the linear approximation approach to derive the model and obtained an analytic solution for steady-state flapping amplitude, energetics, and characteristic frequencies, including natural frequency, damped natural frequency, and peak frequency. It was found that driving the wing at natural frequencies instead of other frequencies maximizes both aerodynamic lift and power efficiency. Interestingly, the flapping velocity is also maximized at the natural frequency, which can lead to an easy experimental approach to identify the natural frequency and validate the resonance design. In other words, achieving resonance in flapping wings

can be recognized as one of the most important principles in enhancing power efficiency, lift generation, and flight control performance of high-frequency flapping wing micro air vehicles (MAVs).

1.3 Insect Flight Modelling

Flying insects show an extraordinary capacity to generate complex aerodynamic forces and navigate through precise and agile movements. This is achieved through an integrated system comprising wings that generate aerodynamic force, muscles that move the wings, and a control system that modulates power output from the muscles.

A majority of the studies on insect flight dynamics [25, 26, 27] have been conducted on the basis of the so-called averaged model[28], assuming that the wing-beat frequency is sufficiently high compared with the insect's natural frequency of body motion. In this case, the variation in periodic aerodynamic and inertial forces at the flapping frequencies will then not exhibit resonance with the body's gross motion (e.g. Shreyas et al[29] showed (Table 1) that for different insects, as size decreases, the flutter frequency increases to produce adequate lift to keep its weight in the air using smaller wings.), and the oscillating forces may be replaced by the average force of the flapping wing cycle. By introducing the averaged model, the equations of motion can be approximated and rewritten as a set of nonlinear ordinary differential equations.[30]. Large insects like hawkmoths with relatively low flapping frequency may not conform to linear theories due to body oscillations that occur on a similar time-scale as flapping wings.[31].

Insect	Wing size(mm)	Frequency
Butterflies	42.7 - 57.3	4-10
Damselfly	18-190	15-20
Dragonfly	50-127	25-40
Beetles	14-25	40-90
Honeybee	9.7	200
Mosquito	2.4-3.3	450-600
Midges	1-3	600-1000

Table 1: Insect flapping frequency

1.3.1 Numerical Modelling

The question regarding the flight mechanics of flapping animals can be explained through investigating the aerodynamic approach and exploring into the fundamental issue of the interaction between the wings and the surrounding air. The flight mechanism is mainly defined by the way that the wings are put into motion, the related characteristics, and the key aspects of the interaction between the wings and the airflow.

With recent advances in computational methods[32], researchers have attempted to solve the insect flight problem using numerical methods, with varying degrees of success. [33, 34, 35, 36, 37]. Liu el at.[38] He established an overall understanding of the viscous and unsteady flow around the flapping wing and of the time course of instantaneous force production, which reveals that hovering flight is dominated by the unsteady aerodynamics of both the instantaneous dynamics and also the past history of the wing. Abel Vargas[39]conducted a thorough study of a pleated wing section based on Aeshna cyanea's wing, using computational fluid dynamics at ultra-low Reynolds numbers that correspond to the dragonflies' gliding

flight. The simulations demonstrate that the pleated airfoil produces comparable and sometimes higher lift than the profiled airfoil, with a drag similar to that of its profiled counterpart. Antonia B. K. [40] utilized the finite element method (FEM) to compute models of a dragonfly wing and a fly wing in order to quantify the quality of material distribution. This method allows ones to take into account for the individual variations in structural parameters, which is particularly helpful when dealing with problems about the stability of a construction.
However, numerical computational fluid dynamics approaches are currently additionally limited by the computing power required for 3-dimensional, unsteady flows at higher Reynolds numbers.
In the hope of finding approximate analytical solutions to the insect flight problem, scientists have developed simplified models based on quasi-steady approximations. Its optimized version, Blade-element technique, found to be effective for propellers and helicopters, have been extended to flapping flight for hovering [41, 42, 43, 44]and ascending[45] birds and insects flight.

1.3.2 Physical modelling

Due to the inherent challenges directly studying insects or finding theoretical solutions to the flight aerodynamics, many researchers have used mechanical models to study insect flight. When constructing these models, the Reynolds number and reduced frequency parameter (body velocity/wing velocity) of the mechanical model are matched to that of an actual insect. This condition, called 'dynamic scaling', ensures that the underlying fluid dynamic phenomena are conserved. William B. Dickson[46] performed a dynamically scaled robotic model equipped with a torque feedback mechanism to study the dynamics of yaw turns in the fruit fly Drosophila melanogaster. David L. [47] present an integrated approach to scale the biological fluid dynamics of a wing that flaps, spins or translates. Both the morphology and kinematics of the locomotory system are coupled to the Navier-Stokes equation, through which they find dimensionless numbers that represent rotational accelerations in the flow due to wing kinematics and morphology. W.B.Lay [48] He present a three-dimensional numerical simulation of a four-wing flapping micro-aerial vehicle (FMAV), known as the Delfly micro. The simulation was performed using an immersed boundary method Navier-Stokes finite volume solver at Reynolds numbers of 5500 (forward flight condition). Results indicates that in comparison to the Delfly II flapping kinematics (a similar FMAV configuration but smaller flapping stroke angles), the Delfly-Micro flapping kinematics provides more thrust while maintaining the same efficiency.

1.4 Numerical Continuation Methods

Numerical continuation methods are essential computational techniques used to analyze the behavior of nonlinear systems by tracking the solutions of differential equations as parameters vary. These methods are particularly valuable in biomechanics and biomimetics, where systems often exhibit complex, nonlinear behaviors due to the intricate interactions within biological tissues and structures. Within the nonlinear dynamics community, numerical continuation methods are standard tools for analyzing nonlinear differential equations.
Biological systems are rarely linear, instead often falling into the broad category of nonlinear systems [49]. Nonlinear systems are typically not analytically tractable, meaning it is generally not possible to obtain a closed-form solution to a nonlinear differential equation. Consequently, the field of nonlinear dynamics focuses on methods to analyse these equations without directly solving them. Despite the challenges, working with nonlinear systems is justified by their immense explanatory power. Classic examples include the work of Hodgkin and Huxley, which laid the foundations of modern neuroscience; the Mackey-Glass equation, which describes the effects of time-delayed feedback on respiratory and hematopoietic diseases; and the Lotka-Volterra model, which explains predator-prey interactions. Nonlinear models and the analysis tools that go with them are used a lot in synthetic biology to design and show gene networks that were made

artificially [50].

The fundamental numerical continuation methods, such as the predictor-corrector (PC) method and the pseudo-arclength (PL) method, are detailed in [51]. These principles are used recently to build a framework to solve continuation and bifurcation problems in nonlinear partial differential equations in [52]. Many nonlinear vibration problems are investigated using continuation methods [53, 54, 55, 56, 57]. Recent studies have explored the nonlinear normal modes of dynamic systems using a shooting algorithm combined with pseudo-arclength continuation [58, 59, 60]. In [61], the harmonic balance and arc-length continuation methods were used to look at how blade disks' free and forced vibrations are not linear in terms of geometry. In 2013, Liao [62] proposed a framework for harmonic balance-based constraint optimisation that looks for the worst-case resonance response while using vibration frequency as an optimisation variable.Liu et al. (2018) combined the shooting method with pseudo-arclength continuation to study the nonlinear dynamics of dielectric elastomers [63].However, the shooting-based continuation method has underlying challenges, such as complexity and simulation time scaling with the system's dimension, making frequency-domain harmonic balance methods appealing. Renault et al.[64] investigated the continuation of antiresonance responses using the harmonic balance method with a continuation technique. Cochelin and Vergez [65] developed a higher-order harmonic balance method for the continuation of periodic motions.

Guillot et.al [66] proposed a Taylor series-based continuation method to compute bifurcation diagrams of nonlinear systems. In this approach, the harmonic balance method is combined with the asymptotic numerical method (ANM) to follow periodic solutions of delay differential equations. ANM requires auxiliary variables and additional equations to express the system in quadratic form, potentially introducing artificial solutions. Moreover, increasing the system's dimension leads to a large number of differential/algebraic equations, posing numerical challenges and computational costs.

The analysis of quasi-periodic motions in nonlinear systems has gained attention in the nonlinear dynamics community [67]. conducted foundational research on the nonlinear dynamics of aperiodic solutions, utilising the double perturbation method for theoretical analysis and the generalised Poincaré map for numerical calculation. With the use of the double perturbation method for theoretical analysis and the generalized Poincare map for numerical calculation, both the analytical and numerical approaches to search quasi-periodic solutions of nonlinear systems are presented in [68]. Jain et al. developed an integral equation approach combining Picard iteration and the Newton-Raphson scheme to approximate periodic or quasi-periodic responses, alleviating intensive numerical integration calculations[69]. Huang et al. [70] studied quasi-periodic solutions of fixed-fixed translating beam equations via the incremental harmonic balance methodology and used Floquet theory to investigate the stability of periodic responses. Liu et al. reported a harmonic balance method to search for quasi-periodic solutions of nonlinear systems [71]. Kim and Noah [72] confirmed quasi-periodic responses in a non-smooth Jeffcott rotor system with bearing clearance. The harmonic balance methodology is extended in [73]to study the localization of quasi-periodic motions in cyclic structures. In order to locate the isolated solutions in the global parameter space, Liao developed a hybrid method incorporating global exploration and local exploitation [74] The harmonic balance technique has been applied successfully for numerical continuation of quasi-periodic solutions [75]focusing on the quasi-periodic response characteristics of piecewise smooth rotor/stator rubbing systems. In [76], a harmonic balance approach is presented for detecting and tracing quasi-periodic solutions with two frequencies, assuming zero initial velocities.

However, the predictor-corrector solver in continuation methods relies on root-finding approaches, raising open questions about the application of Newton-type solvers due to the complex dynamical behaviors of nonlinear systems. During the continuation process, parameters are treated as optimization variables, and prediction techniques are applied to obtain reliable initial guesses corrected via root-finding methods. To apply the root-finding algorithm, the number of nonlinear equations must equal the number of unknowns. When the number of unknown variables exceeds the original equations, additional equations are required, limiting the Newton-type predictor-corrector continuation method. Moreover, efficient tracking of periodic

solutions in multi-parameter nonlinear systems faces obstacles. Continuation methods also encounter difficulties with isolated solution problems [77, 78, 79]. Indeed, the existence of isolated solutions hinders the detection of isolated branches using continuation methods.

2 Optimization Modelling

2.1 System Description

Consider a general 1-DOF nonlinear, time-invariant, parallel elastic actuation (PEA) system:

$$D(x(t), \dot{x}(t), \ddot{x}(t), ...) + F_s(x(t)) = F(t), \tag{2}$$

with time variable t and frequency variable Ω; force input F, kinematic output x, general continuous dynamics $D(\cdot)$, and elastic force $F_s(x)$. Note that $D(\cdot)$ might include additional elastic force alongside $F_s(x)$ [80, 81]. A presents a schematic of this general PEA system, which can be used to model a range of insect and insect-inspired propulsion systems—including, the flight motor of the fruit fly, *Drosophila melanogaster* and the spring-assisted FW-MAV of Chin *et al.* [82].

The mechanical power output of the actuator in Fig. 1(a) is

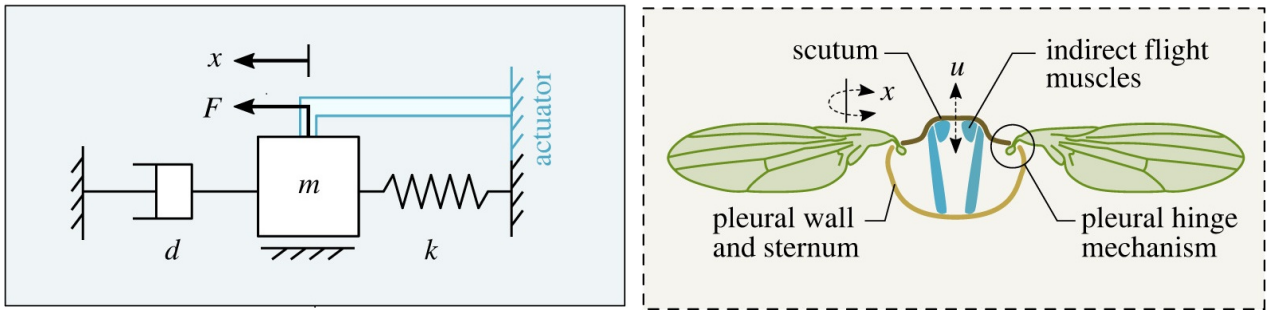

(a) Diagram of a PEA

(b) Flight motor description of Fruit Fly

Figure 1: (a)In this case, the mass m moves with displacement $x(t)$, connecting with a spring of stiffness k; and there is a viscous damper d resists the relative velocity $\dot{x}$ of the mass with force $-d\dot{x}$; (b) is a simplified description of the 'thorex-wing' system of Fruit Fly [81].

$$P(t) = \dot{x(t)}F(t) \tag{3}$$

Instantaneously, this power output can be positive ($P > 0$), negative ($P < 0$), or zero. Positive power output represent the power flow from the actuator to the system, which also indicates that the system energy increases and negative power output, the reverse. Obviously, reducing the level of negative power output increases the system efficiency, in a certain sense: it is inefficient to use the actuator to withdraw energy from the system, *cf.* [83]. In the best possible case, the actuator itself might imperfectly store this energy in an internal potential (*e.g.*, in a regenerative actuator [83]); but in the worst case, the actuator's own power source is consumed in order to withdraw this energy (*e.g.*, as resist power losses in an electromagnetic actuator). This intuition can be formalised [80, 81]: in a wide range of systems, $D(\cdot)$, and kinematics, $x(t)$, the state of non-negative power ($P(t) \geq 0, \forall t$) represents optimality in absolute mechanical power consumption

$$\bar{P}_{\text{abs}} = \int_0^\infty |P(t)| dt \tag{4}$$

with respect to the elastic force $F_s(x)$. That is, it is impossible to alter the system elasticity, $F_s(x)$, such that $\bar{P}_{\text{abs}}$ is reduced and the same applies to a range of other power consumption metrics, covering the behaviour of a range of physical actuators [80].

The set of periodic states, $x(t) \in \mathcal{X}$, for which this condition is satisfied are the *band-type resonant states*[84]. This set includes the conventional energy resonant (or, global resonant [85]) state, if one exists: the state outputting simple-harmonic motion, $x(t) = \hat{x}\cos(\Omega_e t)$. This frequency, Ω_e, is the system's energy-resonant frequency. However, $x(t) \in \mathcal{X}$ includes also states outputting multiharmonic waveforms with fundamental frequencies (Ω) away from Ω_e: the frequency-band resonant states. In an insect flight motor or FW-MAV, these frequency-band states can enable energy-efficient high-authority control of wingbeat lift forces, via modulation of the wingbeat fundamental frequency (see Section 1.2). In both cases, the frequency band, $\Omega_{\text{min}} \leq \Omega \leq \Omega_{\text{max}}$, over which these states exist determines the authority of this mode of control.
Determining this interval is difficult: it involves searching over all possible periodic waveforms at a given fundamental frequency (Ω) to either find a state with non-negative power or confirm that no such state can exist. As of yet, there are no estimates on the full interval $[\Omega_{\text{min}}, \Omega_{\text{max}}]$ even in linear systems; nor indeed any definitive evidence that the complete set of frequency-band states even forms a single interval in frequency. Numerical approaches to mapping the frequency-band states can address both these knowledge gaps.

2.2 Oscillator Modelling of Flight Motors

As a case study for a numerical method for mapping frequency-band resonance, consider an oscillator (linear model) of a flight motor as approximating the behaviour of a range of insect species [81]. In the time (t) domain:

$$\ddot{x}(t) + 2\xi\omega_0\dot{x}(t) + \omega_0^2 x(t) = f(t), \tag{5}$$

Where

- $x(t)$ is the normalised wing stroke angle ($-1 \leq x \leq 1$, for normative hovering flight);
- $f(t)$ is the muscle or actuator forcing;
- ξ, is the motor damping ratio, accounting for both aerodynamic and structural damping;
- ω_0, the motor natural frequency

Frequency-band states are known to exist within the window:

$$\frac{1}{(\frac{4}{\pi} - 1)\xi + \sqrt{1 + \xi^2)}} \leq \lambda \leq 1. \tag{6}$$

However, the formula in Eq. (6) is derived from analyses with a multi-harmonic waveform with a single parameter—a very coarse approximation of the space of all possible periodic waveforms. To accurately map the space of frequency-band states, a better approximation is needed.

2.3 Waveform

A harmonic waveform Eq. (7) is selected as

$$x(t) = \sum_{k \in \sigma} a_k \cos(k\pi t) \tag{7}$$

and with odd harmonics, $\sigma = \{1, 3, 5, ..., 2N+1\}$; even harmonics, $\sigma = \{1, 2, 4, 6, ..., 2N\}$, or all harmonics; $\sigma = \{1, ..., N\}$; where in each case N is the number of harmonics. The intuition behind this choice is

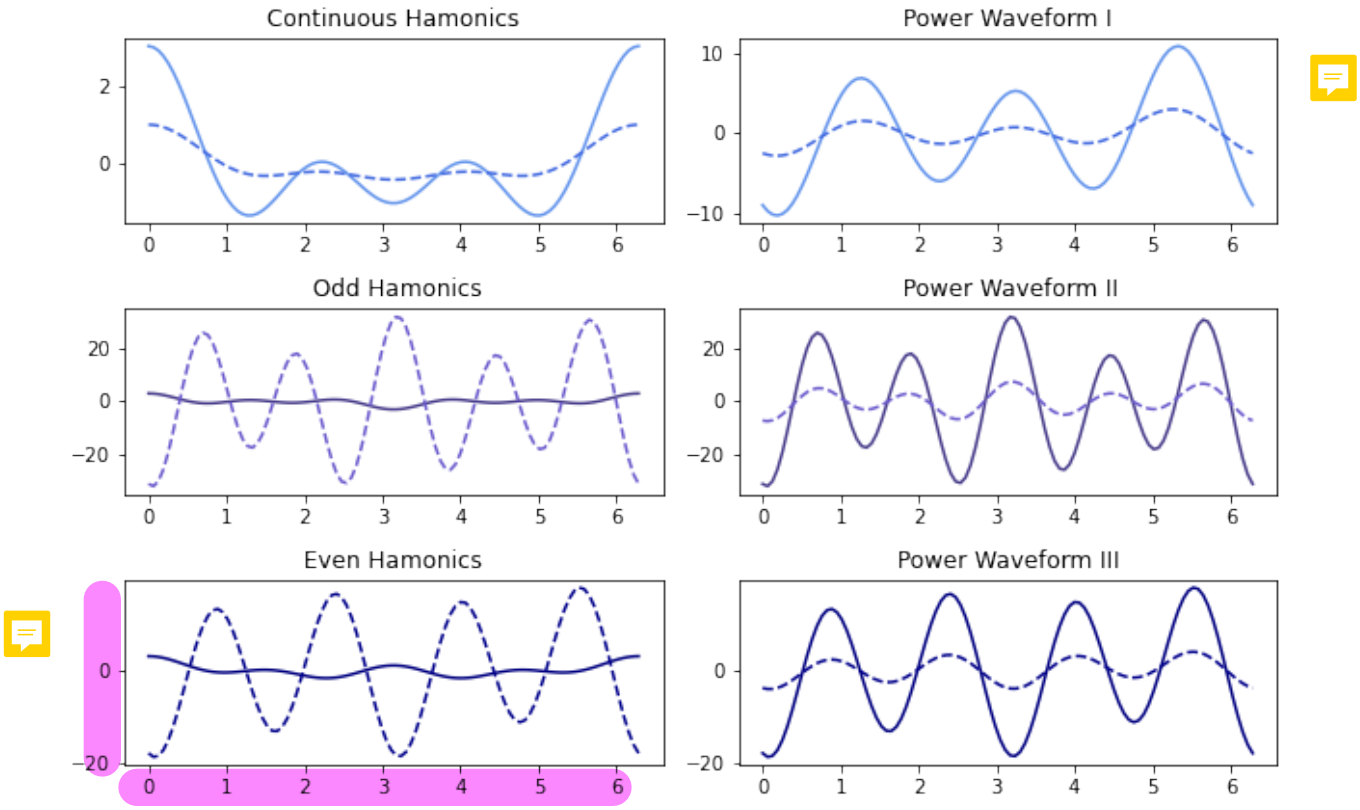

Figure 2: Display of displacement waveform and power waveform in 3 terms case. The left column of figures displays a series of harmonic waveforms: Continuous Hamonics $\sigma = 1, 2, 3$, Odd Harmonics $\sigma = 1, 3, 5$, Even Harmonics $\sigma = 1, 2, 4$. The related power waveforms are displayed in the right column . Solid lines represent the waveforms corresponding to the original harmonics, while dotted lines correspond to tuned harmonics with $\mathbf{A} = [a_1, a_2, a_3] = [0.5, 0.3, 0.2]$.

- These three kinds of harmonics have quite different characteristics. Odd harmonics contribute to the asymmetrical shape of the waveform; Even harmonics contribute to the symmetrical shape of the waveform and continuous harmonics can lead to distortion and alteration of the original waveform's shape. These differences may lead to different characteristics of the corresponding power waveforms.

- We can create any un-typical waveform by combining these three types of harmonics. So, if we can discover an algorithm that applies to all three types of waveforms, it is highly likely that this algorithm can also be applied to atypical waveforms.

2.4 Dynamics of System in Discrete Form

2.4.1 General Discretization

Eq. 5 illustrate a concise dynamics of the system for continuous time derivatives of $x \in \mathbb{R}$. Details about the decomposition of the oscillators are as follows. Noted that for dimensionless problem similar decomposition will also work.
In order to formulate this in an optimization framework, we approximate the continuous-time derivative with a discrete-time representation.

- Discretize time for one period of the reference motion into n time intervals and denote the sample rate (time step length) as Δt.

- Using an Operator $\mathcal{D}$ generate the matrix operation $\dot{x} = \mathcal{D}x$, where $x, \dot{x} \in \mathbb{R}^n$ is the discrete-time representation of x and $\dot{x}$, $\mathcal{D} \in \mathbb{R}^{n \times n}$ is defined as

$$\mathcal{D} = \begin{bmatrix} 1 & 0 & 0 & 0 & \cdots & 0 & 0 \\ -1 & 1 & 0 & 0 & \cdots & 0 & 0 \\ 0 & -1 & 1 & 0 & \cdots & 0 & 0 \\ \vdots & \vdots & \vdots & \vdots & \ddots & \vdots & \vdots \\ 0 & 0 & 0 & 0 & \cdots & -1 & 1 \end{bmatrix} \frac{1}{\Delta t} \tag{8}$$

  $\mathcal{D}x$ is the discrete-time derivative of x based on the first difference method. The first and last rows of D assume that x represents a periodic trajectory, i.e. $x_{t+1} = x_1$, where x_k is the kth element of the displacement vector $\mathbf{x} = [x_1, x_2, \cdots, x_k, \cdots]$.

- Then the equations of motion Eq. 5 can be approximated as

$$\begin{aligned} \mathbf{f} &= \mathcal{D}\mathcal{D}\mathbf{x} + 2\xi\omega_0\mathcal{D}\mathbf{x} + \omega_0^2\mathbf{x} \\ &= (\mathcal{D}^2 + 2\xi\omega_0\mathcal{D} + \omega_0^2)\mathbf{x} \\ &= \mathcal{A}\mathbf{x} \end{aligned} \tag{9}$$

  where $\mathcal{A} = \mathcal{D}^2 + 2\xi\omega_0\mathcal{D} + \omega_0^2 \in \mathbb{R}^{n \times n}$ denote the Operator Stiffness Matrix; $\mathcal{D}^2 \in \mathbb{R}^{n \times n}$ is the matrix that computes the second order derivative; and $\mathbf{f}, \ddot{\mathbf{x}}, \dot{\mathbf{x}}, \mathbf{x} \in \mathbb{R}$ are the discrete-time versions of the muscle force, wing stroke angular acceleration, wing stoke angular velocity and wing stroke angle.

- Similarly, the discretization of power p is given by

$$\begin{aligned} \mathbf{p} &= \mathbf{f}\dot{\mathbf{x}} = \mathcal{B}\mathbf{x} \\ \mathcal{B} &= \mathcal{A}\mathcal{D} \end{aligned} \tag{10}$$

2.4.2 Optimization Algorithm Design

Before delving into the algorithm itself, we must first clarify certain characteristics of the original problem. (Noted, all discussion below is using the continuous harmonics waveform as an example.)
As Eq. 7 given in Section 2.3, waveform $x(t)$ is defined by the amplitude coefficients series $\{a_k\}_1^n$. By rewriting the formula of $x(t)$ into Matrix form, and depicting the corresponding discretization form as

$$\begin{aligned} \mathbf{x} &= \mathbf{AH} \\ \mathbf{A} &= [a_1, a_2, \cdots, a_k, \cdots, a_n] \\ \mathbf{H} &= [\cos \omega\mathbf{t}, \cos 2\omega\mathbf{t}, \cdots, \cos k\omega\mathbf{t}, \cdots, \cos n\omega\mathbf{t}]^{\mathrm{T}} \end{aligned} \tag{11}$$

where $\mathbf{t}$ denotes the interpolated time sequences, $\mathbf{A}$ is defined as the amplitude Matrix and $\mathbf{H}$ is defined as the suffix-harmonic Matrix. The trigonometric form of elements in the suffix-harmonic Matrix gives a convenient way to replace the tedious decomposition process described in Section 2.4 into a series of much simpler trigonometric derivative steps

$$\begin{aligned} \ddot{\mathbf{x}} &= \mathbf{A}\ddot{\mathbf{H}} \\ \dot{\mathbf{x}} &= \mathbf{A}\dot{\mathbf{H}} \\ \mathbf{A} &= [a_1, a_2, \cdots, a_k, \cdots, a_n] \\ \ddot{\mathbf{H}} &= -[\omega^2 \cos \omega\mathbf{t}, 4\omega^2 \cos 2\omega\mathbf{t}, \cdots, k^2\omega^2 \cos k\omega\mathbf{t}, \cdots, n^2\omega^2 \cos n\omega\mathbf{t}]^{\mathrm{T}} \\ \dot{\mathbf{H}} &= -[\omega \sin \omega\mathbf{t}, 2\omega \sin 2\omega\mathbf{t}, \cdots, k\omega \sin k\omega\mathbf{t}, \cdots, \omega \sin n\omega\mathbf{t}]^{\mathrm{T}} \end{aligned} \tag{12}$$

Our goal is to determine the frequency band that satisfies the non-negative condition of power p, while simultaneously minimizing the power consumption of the entire system.[86]. Then challenges turn out: (1) the amplitude Matrix $\mathbf{A}$ is completely unknown, (2) the variable to be solved is the frequency ω, which is hidden in the triangular function. This makes it difficult to use common optimization methods, such as linear or nonlinear methods, to solve the objective problem where frequency ω is set up as an optimization variable directly on a time domain. Therefore, we changed our minds a little and transferred the time domain into a $\xi - \omega$ space ($\subset \mathbb{R} \times \mathbb{R}$). We sliced the whole oscillation into n units (where n is defined the same as the definition we given in Section 2.4). Each unit on the mesh-grid $\xi - \omega$ space corresponds to an individual element $t_k \in \mathbf{t}$. Then, we denote the discretization form for a single unit as

$$\begin{aligned} \mathbf{x}_{t_i} &= \mathbf{A}\mathbf{H}_{t_i} \\ \mathbf{A} &= [a_1, a_2, \cdots, a_k, \cdots, a_n] \\ \mathbf{H}_{t_i} &= [\cos \omega\mathbf{t}_i, \cos 2\omega\mathbf{t}_i, \cdots, \cos k\omega\mathbf{t}_i, \cdots, \cos n\omega\mathbf{t}_i]^{\mathrm{T}} \end{aligned} \tag{13}$$

In this way, (after projecting the unit into the $\xi - \omega$ space,) the only uncertain variable to deal with is $\mathbf{A} = [a_1, a_2, \cdots, a_k, \cdots, a_n]$.
The general idea of the optimization strategy can be summarized as follows:

$$\begin{array}{ccc} \text{Objective variables} & \mathbf{A} = [a_1, a_2, \cdots, a_k, \cdots, a_n] \\ \text{maximize} & \text{peak power (min } p) \\ \text{subject to} & \text{Constraints} \end{array}$$

Each set of values of $\mathbf{A} = [a_1, a_2, \cdots, a_k, \cdots, a_n]$ correspondingly defined a set of values of the power p, which means there will also be a paired $p_{\min}$. We defined the space consisting of these p_min as $\mathbb{P}$. The optimization problem will find a solution set defined as

$$\{\mathbf{A} | \min p(\mathbf{A}) \geq \min p(\mathbf{A}^*), \mathbf{A}^* = [a_1^*, a_2^*, \cdots, a_k^*, \cdots, a_n^*], \forall a_k^* \in \mathbb{R}, k = 1, 2, \cdots, n\} \tag{14}$$

The solution to the optimization problem may result in a displacement waveform $x(t)$ with quite a large or small amplitude(see Fig.3(a)), which also has a great impact on calculating the peak power. Thus, we need a constraint to normalize $x(t)$.
We also need to consider the possibility of the optimization model providing a solution set with "bad values".The amplitude coefficients of the high harmonics may be significantly larger than others, which results in (???)). Solutions like this are not qualified. Therefore, we need a constraint to make sure $x(t)$ is dominated by lower harmonics. Thus, use the definition from the above sections, we can write the

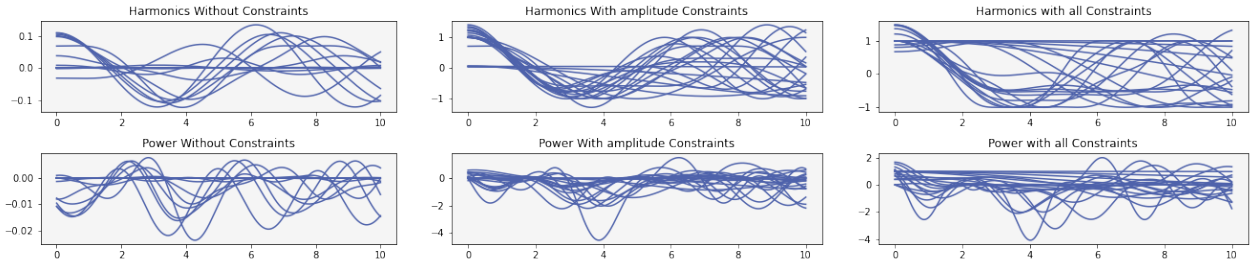

(a) No Constraints (b) Amplitude Constraints (c) Amplitude and Dominance Constraints

Figure 3: The first line of figures shows the displacement waveforms provided by the optimization solver, and the second line of figures shows the corresponding power waveforms. Figure (a) is plotted using solutions given by the optimizer without any constraints. The x(t) we obtained fluctuates over a very small range. Similar things happen to the power p(t). This reduces the accuracy of the optimizer. In Figure (b), by using the normalization constraint, the displacement waveform x(t) has been adjusted to a periodic function on the interval [-1,1]. However, due to the dominance of high harmonics and lack of lower harmonics, the frequency of the solutions waveform of displacement x(t) is quite difficult to be seperated, as is evident in the plot of the power waveform. All these issues are improved when we add the dominance constraint in addition to the amplitude constraint (see Fig.3(c)).

optimisation problem as below

$$\begin{array}{cc} \text{Objective variables} & \mathbf{A} = [a_1, a_2, \cdots, a_k, \cdots, a_n] \\ \text{maximize} & \min p / \max p \\ \text{subject to} & \max(\mathbf{x}) \text{ - } \min(\mathbf{x}) \leq 2 \\ & a_1 > 0.5 \end{array}$$

2.5 Numerical Continuation Algorithm

For any given ξ^*, we can parametrize the function of power p with respect to the parameter

$$\Theta = \frac{\omega}{\omega_0}, \alpha = [a_1, a_2, \ldots, a_m] \tag{15}$$

denoted as $p = p(\Theta, \alpha)$. According to the definition of frequency resonance, the trajectory that truly matters to us is $c_\Theta(\alpha)$, which consists of all Θ^*, α^* that satisfy

$$\min p(\Theta, \alpha) \geq 0 \tag{16}$$

Assume (Θ_1, α_1) and (Θ_2, α_2) are two points on the trajectory $c_\Theta^{\xi^*}(\alpha) = p^{\xi^*}(\Theta, \alpha)$ at $\xi = \xi^*$, with $c_{\Theta_1}^{\xi^*}(\alpha_1) = p(\Theta_1, \alpha_1)$ being known. Similar to the basic principles of classical numerical continuation methods, we use α_1 as the 'predictor' for the approximation value of $p^{\xi^*}(\Theta_2, \alpha_2)$, denoted as

$$\bar{p}^{\xi^*}(\Theta_2, \alpha_2) = p^{\xi^*}(\Theta_2, \alpha_1), \tag{17}$$

and use α_1 as the initial value for the optimization variable in the optimization algorithm. Next, we will briefly provide the reasons for doing so.

As (Θ_1, α_1) is a known solution which fulfils the constraint that the corresponding minimum of the trajectory $\min c^{\xi^*}_{\Theta=\Theta_1}(\alpha_1) = \min p^{\xi^*}(\Theta_1, \alpha_1) \geq 0$. The reason is given below.

Suppose Ω_2 is quite near to Ω_1 so that it can be written as $\Omega_2 = \Omega_1 + \mathrm{h}$ (where h is a sufficiently small step width). Then we can say

$$p^{\xi^*}(\Theta_2, \alpha_1) \simeq p^{\xi^*}(\Theta_1, \alpha_1) + \mathrm{h}(p^{\xi^*}(\Theta_1, \alpha_1))', \tag{18}$$

where $(p^{\xi^*}(\Theta_1, \alpha_1))'$ represents the derivative of $(p^{\xi^*}(\Theta_1, \alpha_1))$ with respect to α_1 at the point (Θ_1, α_1). Thus, we have

$$\min c^{\xi^*}_{\Theta=\Theta_2}(\alpha_1) = \min p^{\xi^*}(\Theta_2, \alpha_1) \simeq \min p^{\xi^*}(\Theta_1, \alpha_1) \tag{19}$$

Although $\min c^{\xi^*}_{\Theta=\Theta_2}(\alpha_1) = \min p^{\xi^*}(\Theta_2, \alpha_1)$ is not ensured to be greater than 0, it will at least be quite 'near' to be non-negative. Therefore, when we use (Θ_2, α_1) as the initial value to find the α_2 that fulfils our aim, it will reduce the time cost of the algorithm and also make sure the solution space we found is smooth.

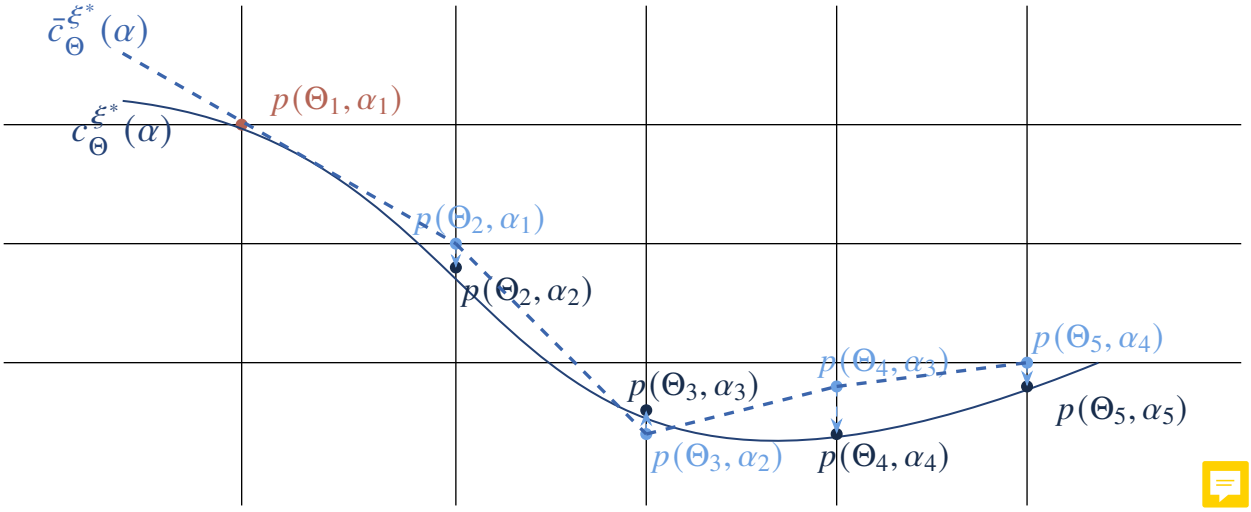

Figure 4: This figure is an illustration of the process that how can we trace the solution trajectory by one known solution $p(\Theta_1, \alpha_1)$. $p(\cdot, \cdot)$ denotes the parametrized power function. Those blue nodes (or 'Guess' solutions) represent the corresponding power function p to those initial values fed to the optimization algorithm and those black nodes represent the final solutions (also parametrized) we found. Then we use $\bar{c}^{\xi^*}_{\Theta}(\alpha)$ to note the trajectory of 'Guess' solutions and use $c^{\xi^*}_{\Theta}(\alpha)$ to note the trajectory of the solutions given by the optimization algorithm.

Because the solutions given by the optimization algorithm are not guaranteed to be non-negative, we still need a filter step at the end of the numerical continuation method. After we use this numerical continuation method to find some numerical solutions, we need to check whether they fulfil the constraint that the minimum of the corresponding power function is non-negative. If they fulfil the constraint, we will add the solution to the solution set, and the corresponding trajectory $c^{\xi^*}_{\Theta}(\alpha)$ will continue. In reverse, if they don't fulfil the constraint, we will break down the corresponding trajectory $c^{\xi^*}_{\Theta}(\alpha)$ and start a new trace process

with a new known solution $p(\Theta_1, \alpha_1)_{\text{new}}$.

Therefore, we have one last problem to solve. According to the description given above, we need an initial solution set that includes enough initial values as the input of the optimization algorithm input. It seems to be hard to find such a set; however, considering the specificity of our work, the simple harmonics can simply fulfil our aim. Thus, the initial solution set, or we can say the 'Guess' solution set consists of these elements where $a_1 = 1$ and $a_i = 0, i = 2, 3, \cdots$. Related proof is given in [84].

As a summary, we are giving the pseudo-code to describe the whole workflow.

Algorithm 1 Workflow with numerical continuation method

Require: Initialization of parameters: Damping Ratio ξ, Natural Frequency ω_0
  for Damping Ratio $\xi \rightarrow$ Defined Domain $[0, \cdots]$ **do**
    while Omega Ratio $\Theta = \frac{\omega}{\omega_0} \rightarrow$ Defined Domain $[1, \cdots]$ **do**
      Initialization: $\alpha = [a_1, 0, \cdots]$;
      Optimization Solver;
      Check the solution given by the solver
      if Solution α^* fulfil the tolerance **then**
        New Initialization for optimization Solver in next iteration: $\alpha = \alpha^*$;
      else if Solution α^* doesn't fulfil the tolerance **then**
        End the current iteration
      end if
      Update Omega Ratio with step width h: $\Theta_{\text{NEW}} = \frac{\omega}{\omega_{0\,\text{NEW}}} = \Theta_{\text{OLD}} + h = \frac{\omega}{\omega_{0\,\text{Old}}} + h$
    end while
  end for

3 Results

For each category, the input damping ratio ξ range from 0 to 1 and omega ratio $\frac{\omega}{\omega_0}$ range from 0 to 2. The choice of this interval is based on the following considerations:

- **Damping ratio ξ Selection**: When the damping ratio ξ exceeds one, the system becomes overdamped. In an overdamped system, the return to equilibrium is slow and lacks oscillatory behaviour, which contrasts sharply with the natural dynamics of insect flight, where rapid and efficient oscillatory motions are essential for manoeuvrability and stability. Therefore, restricting xi to a maximum of 1 ensures the simulation remains representative of real-world insect flight conditions, which typically involve underdamped or critically damped systems for optimal performance.
- **Omega ratio $\frac{\omega}{\omega_0}$ Range Determination (for the example cases)**: The range of the omega ratio $\frac{\omega}{\omega_0}$ is derived from extensive simulation data. Various ranges were tested to determine the most appropriate upper bound. The analysis consistently showed that the extreme values of $\frac{\omega}{\omega_0}$ did not exceed 2 within the solution set. Hence, selecting 2 as the upper limit ensures a comprehensive yet practical range for the simulations, capturing all relevant resonant behaviors without unnecessary computational overhead.

For the example case, the input signal $x(t)$ is modeled as a 3-term polynomial, incorporating odd harmonics. In each simulation, we employed two distinct solver algorithms to find solutions:

- **Active Set Method**: This algorithm is well-suited for solving constrained optimization problems and operates by maintaining a working set of constraints, iteratively adjusting the solution within feasible regions. Its application here helps explore the solution space efficiently, especially in scenarios with complex constraint interactions.

- **Sequential Quadratic Programming (SQP)**: SQP is a powerful optimization technique that solves a sequence of quadratic programming subproblems, converging to a solution that satisfies both the objective function and constraints. Its robustness in handling non-linear problems makes it an ideal choice for this study, providing a valuable comparison against the Active Set method.

The results obtained by each method are compared in the subsequent analysis, highlighting the performance and accuracy differences in solving the objective problems.
For the naive optimization algorithm, we experimented with two approaches for assigning initial values to the vector $\vec{a}$.

- Fixed Initialization of $\vec{a}$: In this approach, the optimization algorithm consistently uses the same initial values for $\vec{a}$, set as $\vec{a} = [0.5, 0.5, 0.5]$. These values are arbitrary and chosen primarily to ensure the optimization solver runs correctly. Although fixed, this initialization provides a baseline for assessing the algorithm's performance and stability under consistent starting conditions.

- Gaussian Sampling: To introduce variability and test the stability of the naive optimization algorithm, we generated s samples (10 samples in the example case, $s = 10$)) using the Gaussian Sampling Method within the vector space $[-1, 1]^m$ (In the example case, the Vector Space is $[-1, 1]^3$).

We compared the results from the naive optimization algorithm with those obtained from the numerical continuation algorithm. Numerical continuation is a technique used to track the solutions of a system of equations as a parameter is varied, providing insights into the system's behavior under different conditions. This comparison allows us to evaluate the efficacy and reliability of the naive optimization algorithm relative to a more established numerical method. We also present the analytical solution in all these figures, which can also give us some information about the accuracy of these numerical algorithms.

3.1 Fixed Initialization vs. Gaussian Sampling

For each element $a_i \in \vec{a}$, we assume $a_i \sim N(\mu, \sigma)$. In the example case, $\mu = 0$. The choice of $\mu = 0$ is based on the symmetrical reference range of a_i (after normalization), which is $[-1, 1]$. This interval is well symmetric about 0, making$\mu = 0$ an appropriate choice considering the properties of the normal distribution. These s (in example case, s = 10) samples serve as initial guesses for each pair $(\xi, \frac{\omega}{\omega_0})$. The algorithm iterates through these samples. Once a solution is found, the corresponding iteration will break. Then the algorithm will subsequently updating $(\xi, \frac{\omega}{\omega_0})$. We provide four groups of samples with different standard deviations ($\sigma = 0.01, 0.5, 1, 2$) and plot the corresponding mapping zones based on the solutions from the naive optimization algorithm with fixed initialization of $\vec{a}$ and the naive optimization algorithm with Gaussian Sampling. These plots will help us to visualize the impact of different initial conditions on the solution space and the stability of the optimization process. Further discussion on these results is presented in the next section.

3.2 Naive Algorithm vs. Numerical Continuation

3.3 Application: Nonlinear System

4 Discussion

5 Conclusion

References

[1] F. Moslem, Z. Babaie, M. Masdari, and K. Fedir, "A review on insects flight aerodynamics, noise sources, and flow control mechanisms," *Proceedings of the Institution of Mechanical Engineers, Part G: Journal of Aerospace Engineering*, vol. 237, pp. 2907–2917, Oct. 2023.

[2] K. D. Jones and M. F. Platzer, "Design and development considerations for biologically inspired flapping-wing micro air vehicles," *Experiments in Fluids*, vol. 46, pp. 799–810, May 2009.

[3] C. H. Greenewalt, "The wings of insects and birds as mechanical oscillators," *Proceedings of the American Philosophical Society*, vol. 104, no. 6, pp. 605–611, 1960. Publisher: JSTOR.

[4] H. Liu, S. Ravi, D. Kolomenskiy, and H. Tanaka, "Biomechanics and biomimetics in insect-inspired flight systems," *Philosophical Transactions of the Royal Society B: Biological Sciences*, vol. 371, no. 1704, p. 20150390, 2016. Publisher: The Royal Society.

[5] J. Gau, N. Gravish, and S. Sponberg, "Indirect actuation reduces flight power requirements in *Manduca sexta* via elastic energy exchange," *Journal of The Royal Society Interface*, vol. 16, p. 20190543, Dec. 2019.

[6] N. T. George, T. C. Irving, C. D. Williams, and T. L. Daniel, "The Cross-Bridge Spring: Can Cool Muscles Store Elastic Energy?," *Science*, vol. 340, pp. 1217–1220, June 2013.

[7] "Biology and physics of locust flight. V. Strength and elasticity of locust cuticle," *Philosophical Transactions of the Royal Society of London. Series B, Biological Sciences*, vol. 245, pp. 137–169, Oct. 1962.

[8] T. Weis-Fogh, "Energetics of hovering flight in hummingbirds and in Drosophila," *Journal of Experimental Biology*, vol. 56, no. 1, pp. 79–104, 1972. Publisher: The Company of Biologists Ltd.

[9] T. Weis-Fogh, "A rubber-like protein in insect cuticle," *Journal of Experimental Biology*, vol. 37, no. 4, pp. 889–907, 1960. Publisher: The Company of Biologists Ltd.

[10] R. Ingersoll and D. Lentink, "How the hummingbird wingbeat is tuned for efficient hovering," *Journal of Experimental Biology*, vol. 221, p. jeb178228, Oct. 2018.

[11] N. Konow, J. A. Cheney, T. J. Roberts, J. R. S. Waldman, and S. M. Swartz, "Spring or string: does tendon elastic action influence wing muscle mechanics in bat flight?," *Proceedings of the Royal Society B: Biological Sciences*, vol. 282, p. 20151832, Oct. 2015.

[12] J. A. Roll, B. Cheng, and X. Deng, "Design, fabrication, and experiments of an electromagnetic actuator for flapping wing micro air vehicles," in *2013 IEEE International Conference on Robotics and Automation*, pp. 809–815, IEEE, 2013.

[13] R. Dudley, *The biomechanics of insect flight: form, function, evolution*. Princeton university press, 2002.

[14] A. Cox, D. Monopoli, D. Cveticanin, M. Goldfarb, and E. Garcia, "The development of elastodynamic components for piezoelectrically actuated flapping micro-air vehicles," *Journal of Intelligent Material Systems and Structures*, vol. 13, no. 9, pp. 611–615, 2002. Publisher: Sage Publications Sage CA: Thousand Oaks, CA.

[15] G. Fischer, A. G. Cox, M. A. Gogola, M. K. Gordon, N. O. Lobontiu, D. J. Monopoli, E. Garcia, and M. Goldfarb, "Elastodynamic locomotion in mesoscale robotic insects," in *Smart Structures and Materials 1999: Electroactive Polymer Actuators and Devices*, vol. 3669, pp. 362–368, SPIE, 1999.

[16] N. O. Lobontiu, M. K. Gordon, G. Fischer, E. Garcia, and M. Goldfarb, "Design and analysis of elastodynamic locomotion for robotic insects," in *Microrobotics and Micromanipulation*, vol. 3519, pp. 118–127, SPIE, 1998.

[17] S. S. Baek, K. Y. Ma, and R. S. Fearing, "Efficient resonant drive of flapping-wing robots," in *2009 IEEE/RSJ International Conference on Intelligent Robots and Systems*, pp. 2854–2860, IEEE, 2009.

[18] Z. A. Khan and S. K. Agrawal, "Design of flapping mechanisms based on transverse bending phenomena in insects," in *Proceedings 2006 IEEE International Conference on Robotics and Automation, 2006. ICRA 2006.*, pp. 2323–2328, IEEE, 2006.

[19] Z. A. Khan and S. K. Agrawal, "Design and optimization of a biologically inspired flapping mechanism for flapping wing micro air vehicles," in *Proceedings 2007 IEEE International Conference on Robotics and Automation*, pp. 373–378, IEEE, 2007.

[20] R. Madangopal, Z. A. Khan, and S. K. Agrawal, "Biologically inspired design of small flapping wing air vehicles using four-bar mechanisms and quasi-steady aerodynamics," 2005.

[21] R. Madangopal, Z. A. Khan, and S. K. Agrawal, "Energetics-based design of small flapping-wing micro air vehicles," *IEEE/ASME Transactions on Mechatronics*, vol. 11, no. 4, pp. 433–438, 2006. Publisher: IEEE.

[22] D. Faux, O. Thomas, S. Grondel, and E. Cattan, "Dynamic simulation and optimization of artificial insect-sized flapping wings for a bioinspired kinematics using a two resonant vibration modes combination," *Journal of Sound and Vibration*, vol. 460, p. 114883, 2019. Publisher: Elsevier.

[23] N. T. Jafferis, M. A. Graule, and R. J. Wood, "Non-linear resonance modeling and system design improvements for underactuated flapping-wing vehicles," in *2016 IEEE International Conference on Robotics and Automation (ICRA)*, pp. 3234–3241, IEEE, 2016.

[24] J. Zhang and X. Deng, "Resonance principle for the design of flapping wing micro air vehicles," *IEEE transactions on Robotics*, vol. 33, no. 1, pp. 183–197, 2017. Publisher: IEEE.

[25] G. Taylor and A. Thomas, "Animal Flight Dynamics II. Longitudinal Stability in Flapping Flight," *Journal of Theoretical Biology*, vol. 214, pp. 351–370, Feb. 2002.

[26] M. Sun and Y. Xiong, "Dynamic flight stability of a hovering bumblebee," *Journal of Experimental Biology*, vol. 208, pp. 447–459, Feb. 2005.

[27] R. Żbikowski, S. A. Ansari, and K. Knowles, "On mathematical modelling of insect flight dynamics in the context of micro air vehicles," *Bioinspiration & Biomimetics*, vol. 1, pp. R26–R37, June 2006.

[28] K. Hohenemser, "Dynamic stability of a helicopter with hinged rotor blades," tech. rep., 1939.

[29] J. Shreyas, S. Devranjan, and K. Sreenivas, "Aerodynamics of bird and insect flight," *Journal of the Indian Institute of Science*, vol. 91, no. 3, pp. 415–427, 2011.

[30] B. Etkin and L. D. Reid, *Dynamics of flight: stability and control*. John Wiley & Sons, 1995.

[31] Y.-L. Zhang, J.-H. Wu, and M. Sun, "Lateral dynamic flight stability of hovering insects: theory vs. numerical simulation," *Acta Mechanica Sinica*, vol. 28, pp. 221–231, Feb. 2012.

[32] S. P. Sane, "The aerodynamics of insect flight," *Journal of Experimental Biology*, vol. 206, pp. 4191–4208, Dec. 2003.

[33] M. J. Smith, P. J. Wilkin, and M. H. Williams, "The advantages of an unsteady panel method in modelling the aerodynamic forces on rigid flapping wings," *Journal of Experimental Biology*, vol. 199, no. 5, pp. 1073–1083, 1996. Publisher: The Company of Biologists Ltd.

[34] H. Liu and K. Kawachi, "A numerical study of insect flight," *Journal of computational physics*, vol. 146, no. 1, pp. 124–156, 1998. Publisher: Elsevier.

[35] Z. J. Wang, "Two dimensional mechanism for insect hovering," *Physical review letters*, vol. 85, no. 10, p. 2216, 2000. Publisher: APS.

[36] R. Ramamurti and W. C. Sandberg, "A three-dimensional computational study of the aerodynamic mechanisms of insect flight," *Journal of experimental biology*, vol. 205, no. 10, pp. 1507–1518, 2002. Publisher: Company of Biologists.

[37] M. Sun and J. Tang, "Unsteady aerodynamic force generation by a model fruit fly wing in flapping motion," *Journal of experimental biology*, vol. 205, no. 1, pp. 55–70, 2002. Publisher: Company of Biologists.

[38] H. Liu, C. P. Ellington, K. Kawachi, C. Van Den Berg, and A. P. Willmott, "A computational fluid dynamic study of hawkmoth hovering," *Journal of experimental biology*, vol. 201, no. 4, pp. 461–477, 1998. Publisher: The Company of Biologists Ltd.

[39] A. Vargas, R. Mittal, and H. Dong, "A computational study of the aerodynamic performance of a dragonfly wing section in gliding flight," *Bioinspiration & Biomimetics*, vol. 3, p. 026004, June 2008.

[40] A. B. Kesel, U. Philippi, and W. Nachtigall, "Biomechanical aspects of the insect wing: an analysis using the finite element method," *Computers in biology and medicine*, vol. 28, no. 4, pp. 423–437, 1998. Publisher: Elsevier.

[41] C. P. Ellington, "The aerodynamics of hovering insect flight. V. A vortex theory," *Philosophical Transactions of the Royal Society of London. B, Biological Sciences*, vol. 305, no. 1122, pp. 115–144, 1984. Publisher: The Royal Society London.

[42] M. Osborne, "Aerodynamics of flapping flight with application to insects," *Journal of Experimental Biology*, vol. 28, no. 2, pp. 221–245, 1951. Publisher: The Company of Biologists Ltd.

[43] J. R. Usherwood and C. P. Ellington, "The aerodynamics of revolving wings I. Model hawkmoth wings," *Journal of Experimental biology*, vol. 205, no. 11, pp. 1547–1564, 2002. Publisher: Company of Biologists.

[44] J. R. Usherwood and C. P. Ellington, "The aerodynamics of revolving wings II. Propeller force coefficients from mayfly to quail," *Journal of Experimental Biology*, vol. 205, no. 11, pp. 1565–1576, 2002. Publisher: Company of Biologists.

[45] G. N. Askew, R. L. Marsh, and C. P. Ellington, "The mechanical power output of the flight muscles of blue-breasted quail (Coturnix chinensis) during take-off," *Journal of Experimental Biology*, vol. 204, no. 21, pp. 3601–3619, 2001. Publisher: Company of Biologists.

[46] W. B. Dickson, P. Polidoro, M. M. Tanner, and M. H. Dickinson, "A linear systems analysis of the yaw dynamics of a dynamically scaled insect model," *Journal of Experimental Biology*, vol. 213, pp. 3047–3061, Sept. 2010.

[47] D. Lentink and M. H. Dickinson, "Biofluiddynamic scaling of flapping, spinning and translating fins and wings," *Journal of Experimental Biology*, vol. 212, pp. 2691–2704, Aug. 2009.

[48] W. Tay, B. Van Oudheusden, and H. Bijl, "Numerical simulation of a flapping four-wing micro-aerial vehicle," *Journal of Fluids and Structures*, vol. 55, pp. 237–261, 2015. Publisher: Elsevier.

[49] A. Beuter, L. Glass, M. C. Mackey, M. S. Titcombe, S. S. Antman, J. E. Marsden, L. Sirovich, and S. Wiggins, eds., *Nonlinear Dynamics in Physiology and Medicine*, vol. 25 of *Interdisciplinary Applied Mathematics*. New York, NY: Springer New York, 2003.

[50] M. Blyth, L. Renson, and L. Marucci, "Tutorial of numerical continuation and bifurcation theory for systems and synthetic biology," Aug. 2020. arXiv:2008.05226 [q-bio].

[51] E. L. Allgower and K. Georg, *Numerical Continuation Methods*, vol. 13 of *Springer Series in Computational Mathematics*. Berlin, Heidelberg: Springer Berlin Heidelberg, 1990.

[52] H. Uecker, "Continuation and Bifurcation in Nonlinear PDEs – Algorithms, Applications, and Experiments," *Jahresbericht der Deutschen Mathematiker-Vereinigung*, vol. 124, pp. 43–80, Mar. 2022.

[53] P. Ribeiro, "Non-linear forced vibrations of thin/thick beams and plates by the finite element and shooting methods," *Computers & Structures*, vol. 82, pp. 1413–1423, July 2004.

[54] P. Sundararajan and S. T. Noah, "Dynamics of Forced Nonlinear Systems Using Shooting/Arc-Length Continuation Method—Application to Rotor Systems," *Journal of Vibration and Acoustics*, vol. 119, pp. 9–20, Jan. 1997.

[55] G. Dimitriadis, "Continuation of Higher-Order Harmonic Balance Solutions for Nonlinear Aeroelastic Systems," *Journal of Aircraft*, vol. 45, pp. 523–537, Mar. 2008.

[56] P. Ribeiro, "Non-linear free periodic vibrations of open cylindrical shallow shells," *Journal of Sound and Vibration*, vol. 313, pp. 224–245, June 2008.

[57] S. Stoykov and P. Ribeiro, "Periodic geometrically nonlinear free vibrations of circular plates," *Journal of Sound and Vibration*, vol. 315, pp. 536–555, Aug. 2008.

[58] G. Kerschen, M. Peeters, J. Golinval, and A. Vakakis, "Nonlinear normal modes, Part I: A useful framework for the structural dynamicist," *Mechanical Systems and Signal Processing*, vol. 23, pp. 170–194, Jan. 2009.

[59] M. Peeters, R. Viguié, G. Sérandour, G. Kerschen, and J.-C. Golinval, "Nonlinear normal modes, Part II: Toward a practical computation using numerical continuation techniques," *Mechanical Systems and Signal Processing*, vol. 23, pp. 195–216, Jan. 2009.

[60] F. Georgiades, M. Peeters, G. Kerschen, J. C. Golinval, and M. Ruzzene, "Modal Analysis of a Nonlinear Periodic Structure with Cyclic Symmetry," *AIAA Journal*, vol. 47, pp. 1014–1025, Apr. 2009.

[61] A. Grolet and F. Thouverez, "Vibration Analysis of a Nonlinear System With Cyclic Symmetry," *Journal of Engineering for Gas Turbines and Power*, vol. 133, p. 022502, Feb. 2011.

[62] H. Liao and W. Sun, "A new method for predicting the maximum vibration amplitude of periodic solution of non-linear system," *Nonlinear Dynamics*, vol. 71, pp. 569–582, Feb. 2013.

[63] F. Liu and J. Zhou, "Shooting and Arc-Length Continuation Method for Periodic Solution and Bifurcation of Nonlinear Oscillation of Viscoelastic Dielectric Elastomers," *Journal of Applied Mechanics*, vol. 85, p. 011005, Jan. 2018.

[64] A. Renault, O. Thomas, and H. Mahé, "Numerical antiresonance continuation of structural systems," *Mechanical Systems and Signal Processing*, vol. 116, pp. 963–984, Feb. 2019.

[65] B. Cochelin and C. Vergez, "A high order purely frequency-based harmonic balance formulation for continuation of periodic solutions," *Journal of Sound and Vibration*, vol. 324, pp. 243–262, July 2009.

[66] L. Guillot, C. Vergez, and B. Cochelin, "Continuation of periodic solutions of various types of delay differential equations using asymptotic numerical method and harmonic balance method," *Nonlinear Dynamics*, vol. 97, pp. 123–134, July 2019.

[67] M. Guskov, J.-J. Sinou, and F. Thouverez, "Multi-dimensional harmonic balance applied to rotor dynamics," *Mechanics Research Communications*, vol. 35, pp. 537–545, Dec. 2008.

[68] J. Awrejcewicz and W. D. Reinhardt, "Quasiperiodicity, strange non-chaotic and chaotic attractors in a forced two degrees-of-freedom system," *ZAMP Zeitschrift fr angewandte Mathematik und Physik*, vol. 41, pp. 713–727, Sept. 1990.

[69] S. Jain, T. Breunung, and G. Haller, "Fast computation of steady-state response for high-degree-of-freedom nonlinear systems," *Nonlinear Dynamics*, vol. 97, pp. 313–341, July 2019.

[70] J. Huang, W. Zhou, and W. Zhu, "Quasi-periodic motions of high-dimensional nonlinear models of a translating beam with a stationary load subsystem under harmonic boundary excitation," *Journal of Sound and Vibration*, vol. 462, p. 114870, Dec. 2019.

[71] G. Liu, Z. Lv, J. Liu, and Y. Chen, "Quasi-periodic aeroelastic response analysis of an airfoil with external store by incremental harmonic balance method," *International Journal of Non-Linear Mechanics*, vol. 100, pp. 10–19, Apr. 2018.

[72] Y.-B. Kim and S. Noah, "QUASI-PERIODIC RESPONSE AND STABILITY ANALYSIS FOR A NON-LINEAR JEFFCOTT ROTOR," *Journal of Sound and Vibration*, vol. 190, pp. 239–253, Feb. 1996.

[73] F. Fontanela, A. Grolet, L. Salles, and N. Hoffmann, "Computation of quasi-periodic localised vibrations in nonlinear cyclic and symmetric structures using harmonic balance methods," *Journal of Sound and Vibration*, vol. 438, pp. 54–65, Jan. 2019.

[74] H. Liao, "Global resonance optimization analysis of nonlinear mechanical systems: Application to the uncertainty quantification problems in rotor dynamics," *Communications in Nonlinear Science and Numerical Simulation*, vol. 19, pp. 3323–3345, Sept. 2014.

[75] L. Peletan, S. Baguet, M. Torkhani, and G. Jacquet-Richardet, "Quasi-periodic harmonic balance method for rubbing self-induced vibrations in rotor–stator dynamics," *Nonlinear Dynamics*, vol. 78, pp. 2501–2515, Dec. 2014.

[76] L. Guillot, P. Vigué, C. Vergez, and B. Cochelin, "Continuation of quasi-periodic solutions with two-frequency Harmonic Balance Method," *Journal of Sound and Vibration*, vol. 394, pp. 434–450, Apr. 2017.

[77] L. Salles, B. Staples, N. Hoffmann, and C. Schwingshackl, "Continuation techniques for analysis of whole aeroengine dynamics with imperfect bifurcations and isolated solutions," *Nonlinear Dynamics*, vol. 86, pp. 1897–1911, Nov. 2016.

[78] R. Alcorta, S. Baguet, B. Prabel, P. Piteau, and G. Jacquet-Richardet, "Period doubling bifurcation analysis and isolated sub-harmonic resonances in an oscillator with asymmetric clearances," *Nonlinear Dynamics*, vol. 98, pp. 2939–2960, Dec. 2019.

[79] T. Detroux, L. Renson, L. Masset, and G. Kerschen, "The harmonic balance method for bifurcation analysis of large-scale nonlinear mechanical systems," *Computer Methods in Applied Mechanics and Engineering*, vol. 296, pp. 18–38, Nov. 2015.

[80] A. Pons, "The self-oscillation paradox in the flight motor of *Drosophila melanogaster*," *Journal of The Royal Society Interface*, vol. 20, p. 20230421, Nov. 2023.

[81] A. Pons and T. Beatus, "Distinct forms of resonant optimality within insect indirect flight motors," *Journal of The Royal Society Interface*, vol. 19, no. 190, p. 20220080, 2022. Publisher: The Royal Society.

[82] Y.-W. Chin, Z. Ang, Y. Luo, W.-L. Chan, J. S. Chahl, and G.-K. Lau, "Spring-assisted motorized transmission for efficient hover by four flapping wings," *Journal of Mechanisms and Robotics*, vol. 10, no. 6, p. 061014, 2018. Publisher: American Society of Mechanical Engineers.

[83] D. Margolis, "Energy regenerative actuator for motion control with application to fluid power systems," 2005.

[84] A. Pons and T. Beatus, "Band-type resonance: non-discrete energetically optimal resonant states," *Nonlinear Dynamics*, vol. 111, pp. 1161–1192, Jan. 2023.

[85] K. Y. Ma, S. M. Felton, and R. J. Wood, "Design, fabrication, and modeling of the split actuator microrobotic bee," in *2012 IEEE/RSJ International Conference on Intelligent Robots and Systems*, pp. 1133–1140, IEEE, 2012.

[86] A. Pons and T. Beatus, "Elastic-bound conditions for energetically optimal elasticity and their implications for biomimetic propulsion systems," *Nonlinear Dynamics*, vol. 108, pp. 2045–2074, May 2022.